ACS NANO

www.acsnano.org

ARTICLE

Ligand-Free Direct Optical Lithography of Bare Colloidal Nanocrystals via Photo-Oxidation of Surface Ions with Porosity Control

Jia-Ahn Pan, Haoqi Wu, Anthony Gomez, Justin C. Ondry, Joshua Portner, Wooje Cho, Alex Hinkle, Di Wang, and Dmitri V. Talapin*

Cite This: *ACS Nano* 2022, 16, 16067−16076

Read Online

ACCESS | Metrics & More | Article Recommendations | Supporting Information

ABSTRACT: **Microscale patterning of colloidal nanocrystal (NC) films is important for their integration in devices. Here, we introduce the direct optical patterning of all-inorganic NCs without the use of additional photosensitive ligands or additives. We determined that photoexposure of ligand-stripped, "bare" NCs in air significantly reduces their solubility in polar solvents due to photo-oxidation of surface ions. Doses as low as 20 mJ/cm^2 could be used; the only obvious criterion for material selection is that the NCs need to have significant absorption at the irradiation wavelength. However, transparent NCs can still be patterned by mixing them with suitably absorbing NCs. This approach enabled the patterning of bare ZnSe, CdSe, ZnS, InP, CeO_2, CdSe/CdS, and CdSe/ZnS NCs as well as mixtures of ZrO_2 or HfO_2 NCs with ZnSe NCs. Optical, X-ray photoelectron, and infrared spectroscopies show that solubility loss results from desorption of bound solvent due to photo-oxidation of surface ions. We also demonstrate two approaches, compatible with our patterning method, for modulating the porosity and refractive index of NC films. Block copolymer templating decreases the film density, and thus the refractive index, by introducing mesoporosity. Alternatively, hot isostatic pressing increases the packing density and refractive index of NC layers. For example, the packing fraction of a ZnS NC film can be increased from 0.51 to 0.87 upon hot isostatic pressing at 450 °C and 15 000 psi. Our findings demonstrate that direct lithography by photo-oxidation of bare NC surfaces is an accessible patterning method for facilitating the exploration of more complex NC device architectures while eliminating the influence of bulky or insulating surfactants.**

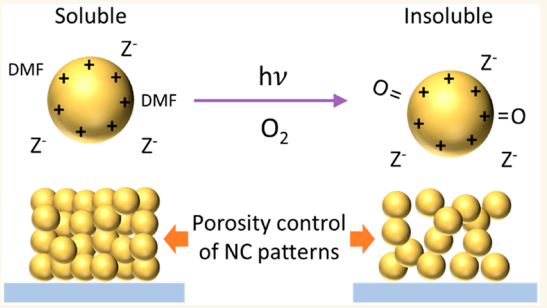

KEYWORDS: *direct optical lithography, colloidal nanocrystals, photo-oxidation, porosity control, refractive index, nanocrystal films, surface ligands*

INTRODUCTION

Colloidal nanocrystals (NCs) have been extensively studied for use in high-performance optoelectronics owing to their useful material properties and solution processability.[1−3] Active layers of NCs in devices such as solar cells, photodetectors, and light-emitting diodes (LEDs) are generally fabricated and tested in the form of continuous thin films. However, the ability to form two-dimensional patterns of NCs is crucial for the assembly of more complex, real-world devices including LED and photodetector arrays,[4,5] multiplexed gas sensors,[6] and nanophotonic elements (e.g., waveguides, diffractive optics, and lasers).[7−9]

There are, accordingly, many well-developed methods for depositing NCs as patterned layers. These include inkjet printing,[10−12] electron-beam lithography,[13,14] transfer printing,[15] nanoimprinting,[16] and photolithography.[17−19] Each of these patterning techniques has its advantages and limitations in terms of cost, scalability, pattern resolution, and generality of approach. In assessing their capabilities, a priority lies in characterizing the surface chemical (ligand) environment of the NCs before and after patterning. In many cases, NCs are patterned in a matrix of long-chain organic ligands or polymer additives. These ligands usually originate from the NC synthesis itself as a necessary component for their solution

Received: April 29, 2022
Accepted: September 12, 2022
Published: September 19, 2022

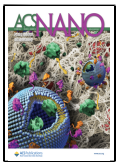

Scheme 1. Patterning Process via Surface Photo-Oxidation of Bare NCs

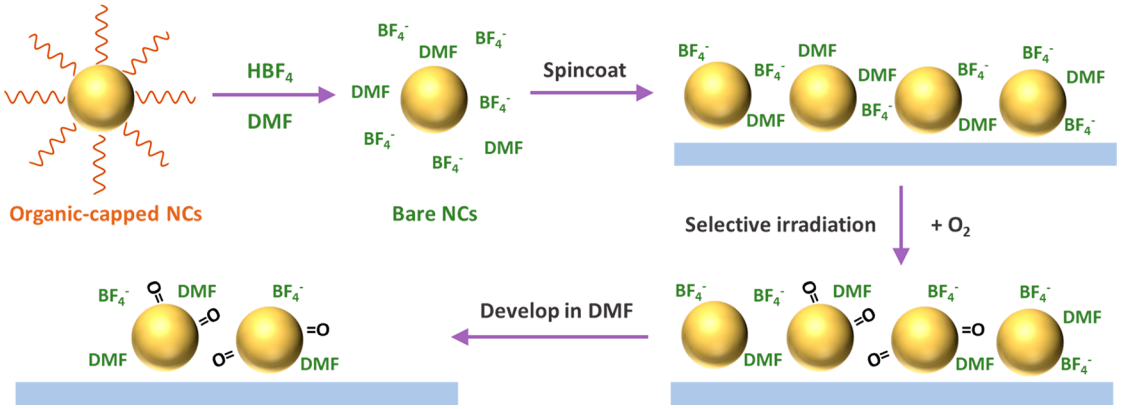

stability, but they limit the NC electronic coupling strength, reduce the stability of the films at high temperatures, and significantly reduce the packing fraction of the NCs in a given volume.

In our lab, we have been developing chemical methods that enable the direct optical lithography of functional inorganic nanomaterials (DOLFIN). This resist-free approach involves identifying suitable photosensitive ligands or additives that modulate the surface charge/polarity of semiconducting, metal oxide, and lead halide perovskite NCs.[5,9,20−22] A key philosophy of our patterning approach is to use additives of very small molecular size to maximize the packing density and electronic coupling in patterned NC films. To this end, it is useful to utilize NCs that have their organic chains removed via ligand stripping approaches, giving "bare" NCs that are charge-stabilized with a noncoordinating anion such as BF_4^-.[23−27] Previously, we have found that "bare" NCs can be patterned by introducing a photoactive chemical compound that reduces the surface charge upon photodecomposition.[9,21] However, the required photoexcitation of electrons need not take place in the sensitizing additive. Another relatively unexplored patterning mechanism utilizes photogenerated holes and electrons in the NCs themselves to drive chemical reactions on the NC surface (such as photo-oxidation), which subsequently changes the NC solubility and effects formation of photopatterns.

The light-induced oxidation of semiconductor NCs has been carefully studied due to the importance of surface chemistry for achieving optimal optoelectronic and luminescent performance. X-ray photoelectron spectroscopy (XPS) of organic-capped CdSe NCs irradiated in air has detected the presence of SeO_2,[28] while optical absorption studies have shown blue-shifting, broadening, and reduction of the excitonic features upon prolonged exposure to light.[29] Similar effects have been found in aqueous dispersions of CdS NCs,[30,31] and the photo-oxidation of InP NCs and nanowires in the presence of HF is a common technique to increase their PL quantum yield.[32−34] In addition, surface oxidation of colloidal nanocrystals can be used to induce oriented attachment to create hierarchical self-assembled structures.[35] Although the photo-oxidation of various NCs can and has been used to create self-assembled hierarchical structures, it has not been used to modulate the NC solubility for direct patterning of arbitrary structures.

Another advantage of using colloidal NCs in devices is the ability to independently control the nano- and mesoscale morphology of the NC films. The crystallinity, crystallite size, and composition of the film can be precisely controlled by using NCs of different size and composition, taking advantage of nearly 30 years of development in the synthesis of colloidal inorganic nanocrystals. Hierarchical structures can be introduced using a variety of thin film modification strategies. For instance, there is a well-developed route to introduce mesoscale porosity into films of bare NCs via polymer templating.[36−40] NCs are mixed with micelles made of amphiphilic block copolymers, then deposited as a film that consists of NCs assembled around the micelle template; removal of this template gives an open porous network of NCs. On the other hand, postprocessing methods such as thermal annealing and hot isostatic pressing can be used to decrease the NC film porosity and allow for further densification of NC films. These approaches have yet to be integrated with strategies for lithographic patterning of nanocrystal films. Such a development would enable applications which simultaneously require hierarchical mesoscale structures and microscale patterned elements such as porous waveguides,[41,42] multiplexed gas sensors,[6] and diffractive optical elements with refractive index tunability.[43,44]

Here, we describe the scope, performance, and chemical mechanisms of ligand-free direct optical lithography of colloidal NCs through the photo-oxidation of surface ions. The native NC ligands from the original colloidal synthesis are first stripped by a strong acid, such as HBF_4 in DMF, to yield electrostatically stabilized "bare" NCs. The NCs are deposited as a film and irradiated to induce local photo-oxidation of surface atoms on portions of the film, which remain insoluble upon development with DMF. High-quality and high-resolution (~1 μm feature sizes) patterns are achievable using ZnSe-BF_4 NCs and 405 nm light exposure. This approach is easily generalized to other II−VI, III−V, and metal oxide NCs. Mixtures of NCs can be used to tune composition of the pattern layers or to pattern materials that are transparent at the desired illumination wavelength. For example, ZnSe NCs can be used as a sensitizer to enable the patterning of visibly transparent NCs such as HfO_2 and ZrO_2 NCs with 405 nm light. The results of ultraviolet−visible optical absorption, X-ray photoelectron, and Fourier transform infrared spectroscopies indicate that this patterning works by the oxidation of surface ions (e.g., Se^{2-} is oxidized to SeO_2), which causes the desorption of bound DMF ligands. Finally, we demonstrate methods to tune the porosity of patterned NC film through block copolymer templating and hot isostatic pressing.

https://doi.org/10.1021/acsnano.2c04189
ACS Nano 2022, 16, 16067−16076

RESULTS AND DISCUSSION

The patterning process via photo-oxidation is shown in Scheme 1. Colloidal NCs capped with long-chain organic ligands are first synthesized by literature methods. The organic ligands are then removed through a single-phase ligand exchange by adding HBF_4 in DMF to colloidal NCs dispersed in toluene, causing the NCs to immediately precipitate out. To remove the displaced organic ligands and excess ions, the NCs are washed several times by dissolving them in DMF and reprecipitating them with toluene. The bare NCs are finally dispersed in DMF with a concentration of about 5−10 wt % (50−100 mg/mL).

The bare NCs are then deposited as a thin film by spin coating, and the film is immediately irradiated selectively using a photomask and a suitable light source (405 nm light for most NCs, 254 nm for ZnS NCs). This leads to the local photo-oxidation of surface ions of the irradiated NCs, reducing their solubility. The film is then developed in DMF, removing unexposed areas while leaving the irradiated NCs behind as a patterned layer.

Microscale patterns of 3 nm ZnSe-BF_4 NCs obtained through the photo-oxidation process are shown in Figure 1.

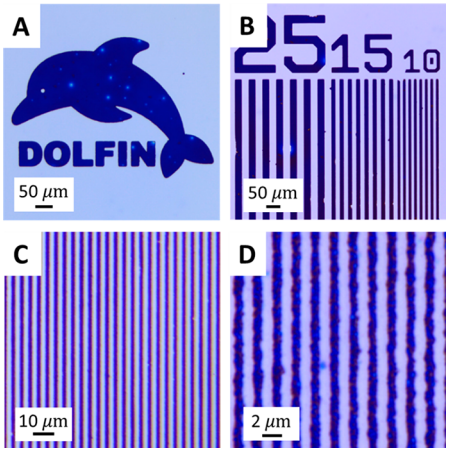

Figure 1. Optical microscope images showing patterns of ZnSe-BF_4 NCs obtained by photo-oxidation patterning.

The optical microscope images show uniform layers with a pattern resolution down to 2 μm and feature sizes as small as 1 μm (the smallest feature of our photomask). The generality of this approach is demonstrated by the patterning of various types of NCs and changing the identity of the counterion. For instance, the patterning process also works for ZnSe NCs that have been stripped with triflic (trifluoromethanesulfonic) acid instead of HBF_4 (Figure 2A). This suggests that the patterning process is not exclusive to the chemistry of a specific counterion. We also show the patterning of other bare semiconductor and oxide NCs such as 4 nm CdSe, 6 nm ZnS, 4 nm InP, 2 nm CeO_2 (Figure 2B−D). Optical properties were preserved; we found, for example, that the position and shape of the photoluminescence (PL) peak of the CdSe-BF_4 NCs do not change appreciably upon irradiation (Figure S1). We also were able to pattern photoluminescent core−shell NCs, including 9 nm CdSe/ZnS NCs and CdSe/CdS dot-in-rod (2 nm × 10 nm) NCs (Figure 2E,F). Although the required patterning dose changes depending on the identity of the NCs, the successful patterning of all these NCs shows that the technique of solubility modulation by photooxidation should be extendable to other types of NCs with only a modest investment of optimization time. The only obvious requirement for successful patterning is that the NCs must have significant absorption at the irradiation wavelength.

To a certain extent, even transparency can be overcome as an obstacle; for some bare NCs that were not patternable on their own, we were able to overcome this limitation by mixing them with NCs that were patternable. For instance, visually transparent HfO_2 nanorods (12 nm by 3 nm) and 3 nm ZrO_2 NCs can be patterned with 405 nm light by mixing in about 25 wt % of 3 nm ZnSe NCs as a sensitizer (Figures 2H and S2A). The quality and resolution of the patterns remain good as shown by the patterning of 1 μm features (Figure 2H, inset), although a significantly higher dose (~1.8 J/cm^2) is required. A final exceptional case is worth mentioning: a particular batch of 8 nm core−shell CdSe/CdS-BF_4 NCs were difficult to pattern on their own through this approach despite their strong absorption at the chosen wavelength. This was due to the irreversible aggregation of these NCs upon spin-coating, leading to insoluble films even without irradiation. We hypothesize that this is due to unoptimized surface chemistry that decreases the electrostatic repulsion between the NCs. However, we show that these CdSe/CdS-BF_4 NCs can still be patterned by mixing them with ZnSe-BF_4 NCs (Figure S2B). The ZnSe-BF_4 NCs help enable patterning by serving as a spacer that prevents the irreversible aggregation of the CdSe/CdS-BF_4 NCs.

We also investigated the pattern quality achieved through this approach in terms of the line-edge roughness, surface roughness, and thickness. The line-edge roughness for a pattern of ZnSe NCs was evaluated through top-down and cross-sectional SEM and found to be on the order of tens of nanometers (Figure S3). We note that this roughness is a convolution of many components of our lithographic process including the roughness of the exposure mask. The surface roughness of the film was estimated to be about 14 nm (Figure S4A), which is a likely a function of the spin-coating conditions and could potentially be further improved by optimizing the spin speed, additives, solvents, etc. In terms of thickness, we successfully patterned ZnSe NC films with thicknesses up to 400 nm (Figure S5). However, spin-coating films at these thicknesses can be challenging due to the formation of cracks. The theoretical thickness should be limited by the penetration of light into the film, which we estimated for ZnSe NCs to be about 1 μm with 405 nm light exposure (Figure S6). If the exposure wavelength can be changed, the light penetration length can be tuned based on the absorption coefficient. Hence, thicker patterns should be attainable with further optimization of the spin-coating parameters, the use of other deposition techniques (e.g., doctor-blading, spray-coating), and the possible addition of plasticizers to prevent cracking.

Although we could pattern any of the inorganic NCs here, there are several requirements we have empirically determined for achieving high-quality patterns through this approach. First, it is important that nonirradiated NCs remain sufficiently spaced apart prior to the development step to avoid getting trapped in the deep primary minimum of a Derjaguin−Landau−Verwey−Overbeek (DLVO) potential. In previous patterning approaches using a photosensitive additive, the unirradiated additive molecule/ions play the role of spacers between NCs, preventing their irreversible aggregation by van der Waals forces.[21] In this ligand-free approach, this role falls on the DMF molecules that are adsorbed on the NC surface as

https://doi.org/10.1021/acsnano.2c04189
ACS Nano 2022, 16, 16067−16076

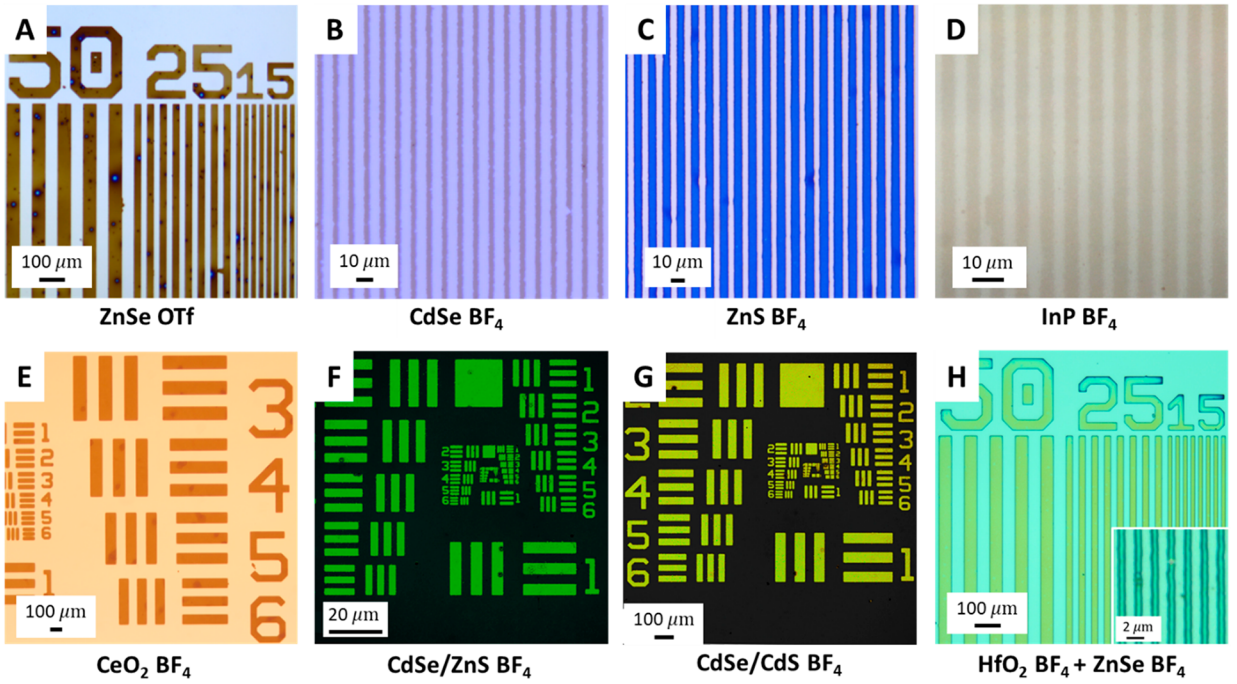

Figure 2. Optical microscope images of patterns made of various NCs and counterions. (A) Patterns of ZnSe NCs with triflate (OTf^-) counterions. (B–G) Patterns of CdSe NCs, ZnS NCs, InP NCs, CeO_2 NCs, CdSe/ZnS NCs, and CdSe/CdS dot-in-rod NCs with BF_4^- counterions. (H) Patterns of HfO_2 NCs mixed with ZnSe NCs (as the sensitizer).

L-type ligands, as previously studied.[23,26] The downside of this is that DMF slowly desorbs from the NC surface over time, leading to the irreversible aggregation and insolubility of the whole film after a certain period of time. Hence, it is important that the deposited NC film is promptly irradiated and developed to prevent this from occurring. Alternatively, this issue should be mitigated by controlling the saturation of DMF in the atmosphere or by including an L-type ligand with higher boiling point or stronger binding affinity to the NC surface.

Another unexpectedly important parameter in this process is the number of washing cycles after ligand stripping, which dictates how many free ions remain in the solution (and in the deposited film). We found that the highest sensitivity was achieved when the NCs were washed extensively (more than 6 rounds of DMF/toluene washing). We hypothesize that this also relates to a spacing effect: excess free ions also serve as a spacer that keeps NCs apart, increasing their solubility. This weakens the effect of photo-oxidation aggregation and reduces its sensitivity. With extensive washing, doses as low as 90 mJ/cm^2 and 20 mJ/cm^2 were sufficient to pattern ~100 nm thick film of ZnSe NCs and ZnS NCs, respectively. These doses are comparable to other DOLFIN approaches that utilize photosensitive ligands or additives[9,21] and comparable to or lower than the dosage required for patterning commercial polymer photoresists.[45]

To elucidate the patterning mechanism, we investigated changes to the NCs during the photoirradiation process. Ultraviolet–visible optical spectroscopy showed a small blue-shift and reduction in intensity of the first absorption peak of ZnS, CdSe, and ZnSe NCs stabilized with BF_4^- in DMF upon irradiation with light (Figure 3A–C). This is consistent with previous reports on the photo-oxidation of colloidal NCs.[29,31] We also found that the photodegradation is much more significant for bare NCs compared to organic-capped NCs (Figure S7). This is reasonable since bare NCs lack the protecting organic ligands that can prevent oxygen from interacting with the NC surface. No significant change to the absorption features is observed upon the irradiation of, for example, ZnSe-BF_4 NCs in a nitrogen atmosphere (Figure 3D). To conclusively demonstrate the importance of oxygen for this patterning mechanism, we carried out a control

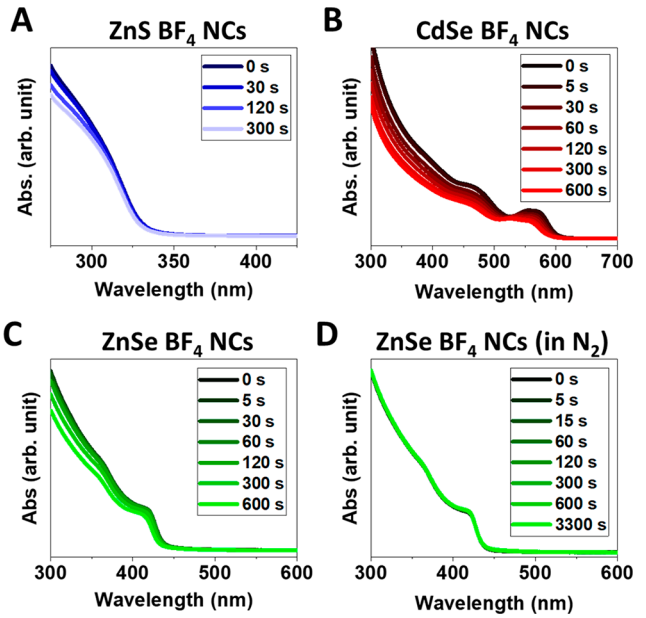

Figure 3. Changes in the NC optical absorption spectra upon light exposure. A 254 nm light source (~6 mW/cm^2) was used to irradiate ZnS NCs (A), while a 405 nm light (~30 mW/cm^2) source was used for CdSe and ZnSe NCs (B–D). Exposures done in air (A–C) showed a clear blue-shift in the spectra, while exposure in a nitrogen atmosphere (D) shows no pronounced changes to the spectra.

https://doi.org/10.1021/acsnano.2c04189
ACS Nano 2022, 16, 16067–16076

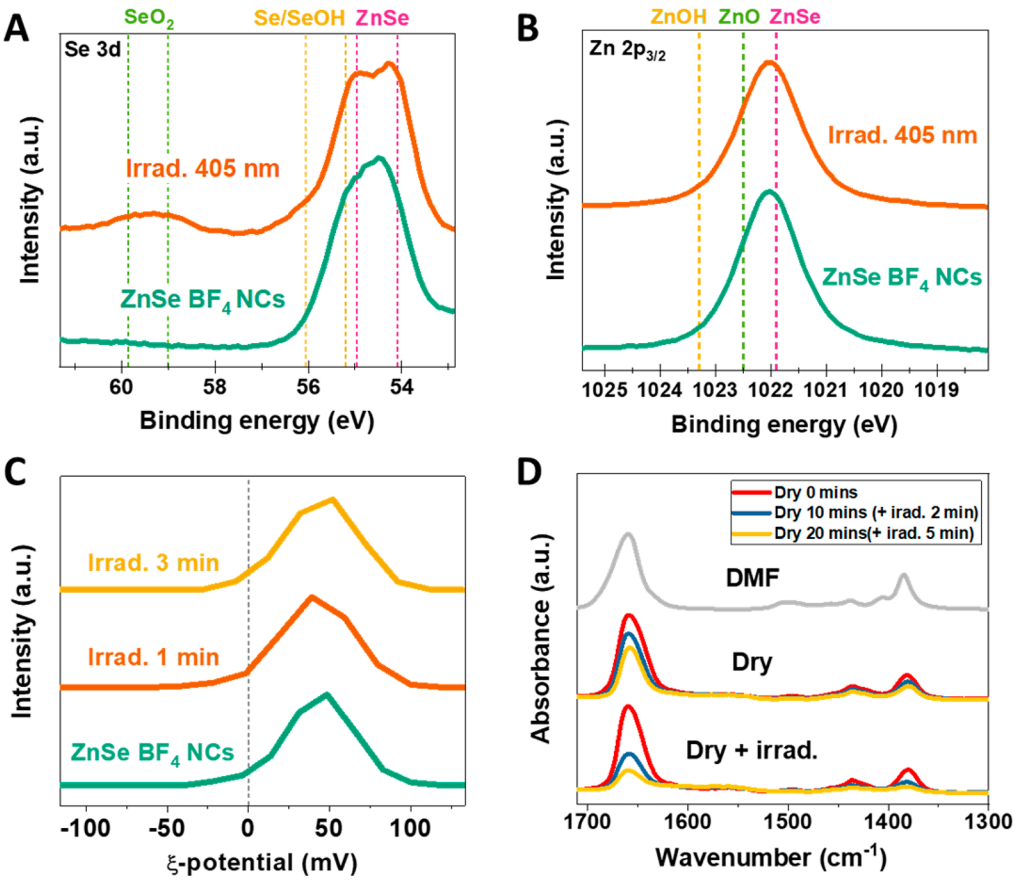

Figure 4. Further investigation of the pattering mechanism via photo-oxidation. (A, B) XPS spectra of the Se 3d and Zn $2p_{3/2}$ regions for ZnSe-BF_4 NCs before and after irradiation. (C) ζ potential measurements of ZnSe-BF_4 NCs after various irradiation times with 405 nm light. (D) FTIR spectra of a ZnSe-BF_4 NC film before and after irradiation with 405 nm light and drying at ambient conditions (bottom three spectra). As a comparison, the spectra of a ZnSe-BF_4 NC film with the same durations of drying time (but without irradiation) were also measured (middle three spectra). A reference DMF spectrum is also shown (top spectrum).

experiment where we irradiated a ZnSe-BF_4 NC film in a nitrogen atmosphere (Figure S8). Irradiation in air-free conditions did not result in a solubility change of the ZnSe-BF_4 NC film even at a high dose (~1.8 J/cm^2, 60 s exposure time). In contrast, an exposure dose of 0.15 J/cm^2 to a similar ZnSe NC film in air leads to a clear reduction of colloidal solubility.

We also carried out X-ray photoelectron spectroscopy (XPS) to measure changes in the chemical bonding of surface ions (Figure 4A,B). Before irradiation, the Se 3d region of ZnSe-BF_4 NCs show peaks that can be primarily attributed to ZnSe (Se $3d_{5/2}$, 54.10 eV; Se $3d_{3/2}$, 54.96) and potentially a small amount of Se/SeOH (Se $3d_{5/2}$, 55.20 eV; Se $3d_{3/2}$, 56.06).[46] Upon irradiation, new peaks in the Se 3d region were observed (Se $3d_{5/2}$, 59.0 eV; Se $3d_{3/2}$, 59.86) that correspond to SeO_2, consistent with previous reports.[28,46,47] There is also a perceptible increase in the Se/SeOH peaks upon irradiation. These observations are consistent with the photo-oxidation of surface Se^{2-} ions into several different oxidation species. On the other hand, we do not observe any noticeable change in the oxidation state of Zn based on the XPS spectra for the Zn $2p_{3/2}$ level, which is known be sensitive to the chemical environment of Zn.[46]

Optical absorption, XPS, and oxygen-free patterning control experiments all point toward a photo-oxidation-induced solubility change of NCs. However, they do not directly reveal the mechanism by which photo-oxidation changes the fundamental colloidal interactions that lead to this solubility change. To clarify this, we carried out ζ potential and Fourier transform infrared (FTIR) spectroscopic studies to further probe the changes in the colloidal and surface chemistry upon photo-oxidation. Interestingly, the measured ζ potential of the NCs during this photoaggregation process was mostly unchanged at about +50 mV (Figure 4C), even though significant aggregation was observed in the dynamic light scattering spectra (Figure S9). This is in contrast with other patterning approaches that show the reduction of the ζ potential due to neutralization of the surface charge.[9] Hence, the aggregation of NCs by photo-oxidation does not seem to stem from the neutralization of the positive surface charges.

FTIR spectroscopy was also used to investigate changes in the ligand chemistry. We were particularly interested in observing the effects of photo-oxidation on the surface-bound DMF ligands. Since DMF ligands slowly desorb from the NC upon drying in air, we compared the FTIR spectra of a ZnSe-BF_4 NC film that was dried and irradiated to another NC film that was dried for the same amount of time (Figure 4D and Figure S10). Our results indicate that photoirradiation significantly increases the desorption rate of DMF as shown by the significantly larger decrease in the DMF FTIR peaks (1659 cm^{-1}, 1497 cm^{-1}, 1436 cm^{-1}, 1382 cm^{-1}) for the NC film that was both irradiated and dried compared to NC film that was only dried. The difference was particularly stark after the first 2 min of irradiation, which indicates that most of the

https://doi.org/10.1021/acsnano.2c04189
ACS Nano 2022, 16, 16067−16076

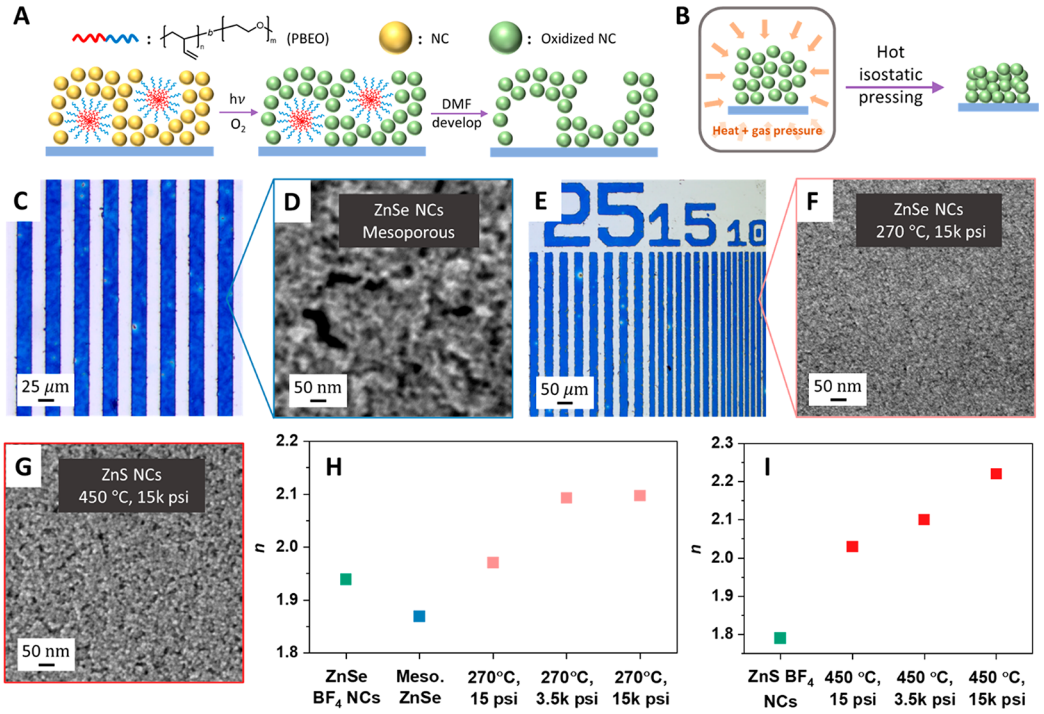

Figure 5. Tuning the porosity and refractive index of patterned ZnSe NC films. (A) Scheme showing a film of NCs mixed with poly(1,2-butadiene)-*b*-poly(ethylene oxide) (PBEO), followed by photo-oxidation patterning and development to produce a mesoporous patterned film. (B) Scheme showing the hot isostatic pressing (HIP) of NC films. (C, D) Optical microscope and SEM images of a patterned mesoporous ZnSe-BF_4 NC film. The mesoporosity was introduced by adding 14 wt % PBEO to the NC solution. (E, F) Optical microscope and SEM images of patterned ZnSe-BF_4 NCs after hot isostatic pressing at 270 °C and 15 000 psi. (G) SEM image of ZnS-BF_4 NCs after hot isostatic pressing at 450 °C and 15 000 psi. (H) Refractive indices of ZnSe-BF_4 NC films as cast, after mesoporous templating, and after hot isostatic pressing treatments at 270 °C and various pressures. (I) Refractive indices of ZnS-BF_4 NC films as cast and after hot isostatic pressing at 450 °C and various pressures.

photoinduced desorption of DMF happens within that time frame. At the same time, photoirradiation also increases the broad IR absorption feature around 3400 cm^{-1}, which we attribute to the increase in the number of hydroxyl groups on the NC surface, consistent with our XPS data.

To account for all these experimental observations, we propose that the photo-oxidation patterning occurs through a mechanism that involves the desorption of DMF ligands from the NC surface due to steric hindrance by oxidized species. For instance, the oxidation of surface Se^{2-} into bulkier SeOH or SeO_3^{2-} groups blocks the ability of DMF ligands to bind to the surface metal sites, leading to their desorption and the loss of colloidal stability.

Thus, far, we have demonstrated the patterning of all-inorganic NCs by photoinduced solubility changes and studied the mechanism of those changes. To further extend the versatility of this approach, we also investigated ways to tune the microstructural features of these patterned films, such as the film porosity. The porosity of NC films is an important parameter for the functionality of various NC devices. For instance, porosity plays a defining role in the accessibility of the NC surfaces to adsorbates upon deposition, which is crucial for resistive gas sensors and other NC devices. In this case, it is often beneficial to have a higher porosity to allow for quick and efficient gas accessibility to the NC surface sites. For other applications, it is more desirable to have as high an NC packing density as possible. As an example, a dense NC film is desirable for optical applications which benefit from a high refractive index for light confinement (e.g., for waveguides).

Here we demonstrate two approaches to modulate the porosity of patterned NC films. To increase the porosity of our patterned films, we show that our photo-oxidation patterning process is compatible with established routes of introducing mesopores into NC films by polymer templating (Figure 5A).[36−40] In this approach, block copolymer micelles are mixed with the bare NCs in DMF and deposited as a film. Subsequent local irradiation of the NC film leads to the oxidation of the exposed NCs and decrease of their solubility in DMF. Upon development with DMF, both the NCs and polymer in the unexposed parts of the film are fully removed. In contrast, in the irradiated parts of the film, only the polymer is washed away while the templated NCs remain insoluble, forming a patterned mesoporous NC film. This ability to maintain a mesoporous structure that does not collapse indicates that the oxidative photopatterning results in relatively strong interactions between NCs when they are precipitated from solution.

Optical microscopy shows that mesoporous ZnSe NC films can be formed using this method (Figure 5C). Notably, a higher dose of ~2.7 J/cm^2 is required for patterning, which we attribute to the effect of hydrophilic segments of the polymer intercalating between NCs and reducing the photoaggregation efficiency. SEM imaging confirms the presence of 50−100 nm mesopores within the patterned structure (Figure 5D and Figure S11B), which is also consistent with the decrease in the refractive index of the mesoporous film (n = 1.87), which is appreciably lower than that of a standard, nontemplated ZnSe NC film (n = 1.94), as measured by ellipsometry (Figure 5H).

https://doi.org/10.1021/acsnano.2c04189
ACS Nano 2022, 16, 16067−16076

On the other hand, to reduce nanoparticle film porosity, we carried out preliminary experiments on the use of hot isostatic pressing (HIP) to densify patterned NC films (Figure 5B). HIP is a well-established densification technique that uses a combination of elevated temperatures and high gas pressures to remove pores from a material while reducing undesirable deformation caused by nonhydrostatic stresses.[48] We subjected ZnSe-BF_4 and ZnS-BF_4 NC films to HIP at several different temperatures and pressures of N_2 and studied their effect on the film porosity, grain size, and pattern features. Optical microscopy (Figure 5E) showed that a patterned film of ZnSe-BF_4 NCs did not crack or change visibly after HIP at 270 °C and 15 000 psi (1034 bar), and the line edge roughness and surface roughness (12 nm) remained similar (Figures S4B and S12). SEM showed significant densification of the ZnSe NC film upon HIP treatment (Figure 5F) with a notable reduction of the 10−20 nm pores found in untreated ZnSe-BF_4 NC films (Figure S11A).

To quantify the densification of ZnSe NC films by HIP, we measured the changes in the refractive index of the NC films through ellipsometry (Figure 5H). For ZnSe NC films that were annealed at 270 °C, using an isostatic pressure of 3500 psi (241 bar) led to a significantly higher refractive index (n = 2.09) compared to annealing under the standard atmospheric pressure of 15 psi (n = 1.97). However, further increasing the pressure to 15 000 psi yielded no further increase in the refractive index. Moreover, XRD analysis shows no significant increase in the Scherrer domain size of the NCs (2.7 nm) after HIP at 270 °C and 15 000 psi (Figure S13A). This indicates that the densification is due to a reduction in porosity rather than grain growth.

We also measured changes in the refractive index of ZnS NC films after HIP at 450 °C. Our results show a similar increase in the refractive index with increasing pressure (Figure 5I). In this case, however, we found that annealing a spin-coated ZnS NC film (n = 1.79, as cast) with a pressure of 15 000 psi yielded the highest refractive index (n = 2.22) compared to annealing under standard pressure (n = 2.03) or at 3500 psi (n = 2.10). Both SEM and XRD showed that HIP treatment at 450 °C and 15 000 psi led to an increase in grain size, with an increase in the Scherrer size from 6.2 to 7.1 nm (Figure 5G and Figure S13B). Hence, densification in this scenario is also aided by grain growth of the NCs.

To determine the porosity of the film from its refractive index, we can use effective medium models. One model which works well for nonabsorbing nanoporous films is the model that applies the volume averaging theory (VAT) to Maxwell's equations.[49,50] According to this model, the volume fraction, ϕ, of the dispersed phase is given by

$$\phi = \frac{n_{\mathrm{eff}}^2 - n_{\mathrm{c}}^2}{n_{\mathrm{d}}^2 - n_{\mathrm{c}}^2}$$

where n_{d} is the refractive index of the dispersed phase, n_{c} is the refractive index of the continuous phase, and n_{eff} is the measured effective refractive index. For ZnSe NC films, n_{d} = 2.578 (the bulk refractive index) and n_{c} = 1 (air). After HIP at 270 °C and 3500 psi, we have n_{eff} = 2.09, resulting in a NC volume fraction of ϕ = 0.60. This is considerably larger than the volume fraction of as-cast NC films (ϕ = 0.49). For ZnS NC films, the bulk refractive index is n_{d} = 2.35. Applying HIP treatment at 450 °C and 15 000 psi results in the refractive index of n_{eff} = 2.22, which gives a packing fraction of ϕ = 0.87. This is much higher than the packing fraction of as-cast ZnS NC films (ϕ = 0.51). Thus, hot isostatic pressing can increase the packing fraction of NCs by as much as 0.36.

We have shown that the porosity of patterned NC films can be tuned by block copolymer templating and HIP. Future work involves exploring a wider temperature and pressure range used in the HIP process. This may enable grain growth and further densification of the NC films to approach the refractive index of bulk inorganic materials. On the other hand, the mesoporosity of the NC film may be further optimized by tuning the amount of polymer added as well as the chemical interactions between NC surface and the polymer.[36,37]

CONCLUSIONS

In summary, we demonstrate the direct optical lithography of ligand-stripped, all-inorganic colloidal NCs via the photo-oxidation of surface ions. We show the high-quality patterning of a variety of NCs such as ZnSe, CdSe, CdS, InP, and CeO_2 NCs, as well as mixtures of NCs. We also probed the chemical changes induced during the patterning process, and our results are consistent with the photo-oxidation of surface ions by oxygen, leading to the desorption of DMF and the aggregation of NCs. Finally, we show that polymer templating and hot isostatic pressing are viable approaches to modulate the porosity and refractive index of the patterned NC films. These additional knobs for porosity control extend the versatility of colloidal NCs in nanophotonic and gas sensing applications.

METHODS

Ligand Stripping of NCs. Colloidal ZnSe, ZnS, CdSe, ZrO_2, HfO_2, CdSe/CdS, and CdSe/ZnS NCs with organic ligands were synthesized according to modified recipes from prior reports. More details on the syntheses can be found in the Supporting Information. InP NCs were obtained from Nanosys and used after precipitation with ethanol, centrifugation, and resuspension in toluene.

HBF_4 in DMF (5 wt %, 0.57 M) was prepared by adding HBF_4−diethyl ether complex solution dropwise to DMF with a volume ratio of 1:9 (*caution: vigorous reaction*). About 0.1 mL of this HBF_4 solution was added to a solution of organic-capped NCs dispersed in 1 mL of toluene (~20 mg/mL). The addition of acid immediately induced the precipitation of the NCs. After vortex mixing for 20 s, the NC suspension was centrifuged. The supernatant was discarded, and the NC residue was washed 3−6 times by dissolving it in DMF and precipitating it with toluene, depending on the type of NC. (For ZnSe NCs, 6 washing cycles were done, each involving 0.5 mL of DMF followed by ~1.5 mL of toluene.) After washing, the NCs were finally dispersed in DMF at a concentration of about 50−100 mg/mL. This ligand-stripping procedure could be scaled up by a volume factor of 10 without any apparent effect on the colloidal stability. For ligand-stripping with triflic (trifluoromethanesulfonic) acid, the same procedure was used, replacing the HBF_4 solution with triflic acid dissolved in DMF (0.5 M).

Photo-Oxidation Patterning. Silicon wafers with a native oxide layer were cut into 1 in. × 1 in. substrates and sonicated in acetone (5 min) and ethanol (5 min), then cleaned with oxygen plasma for about 10 min. The bare NCs were deposited onto the substrate by spin-coating. The substrate, with the NC film facing up, was then placed on a glass slide. A patterned chrome mask, with the mask layer facing down, was then placed on top of the substrate. Two binder clips were then used to hold the stack together. This stack was then exposed to 405 nm light (M405LP1-C1, Thorlabs, measured power density of ~30 mW/cm^2) or a low-pressure mercury vapor grid lamp emitting at 254 nm (~6 mW/cm^2, Jelight Company, Inc.). After exposure, the substrate was immersed into a DMF developer for ~10 s and then dried with a N_2 gun. Patterns of mixtures of bare NCs were obtained

https://doi.org/10.1021/acsnano.2c04189
ACS Nano 2022, 16, 16067−16076

by vortex mixing of two different NC solutions before using the same patterning procedure as above.

Patterning of Mesoporous NC Films. Poly(1,2-butadiene)-*b*-poly(ethylene oxide) (PBEO) with a mass ratio of PB(5200)-*b*-PEO(4500) was dissolved in DMF (2.5 wt %) and stirred for a few hours at room temperature. The PBEO solution was then added to a ZnSe NC-BF_4 solution to obtain 14 wt % of PBEO with respect to the mass of NCs. After vortex mixing, the PBEO-ZnSe NC-BF_4 mixture was patterned according to the same procedure as above.

Hot Isostatic Pressing (HIP) of NC Films. Unpatterned or patterned ZnSe-BF_4 NC films on Si or glass substrates were placed in a stainless-steel reactor, which was pressurized at room temperature with ultrahigh purity N_2 gas and a pressure booster to a precalculated pressure (e.g., 8000 psi) to reach the desired pressure (e.g., 15 000 psi) at the set heating temperature (e.g., 270 °C). The sealed reactor was then heated to the set temperature, which also led to an increase in pressure to the desired pressure. The HIP treatment was carried out for 16 h, after which the reactor was cooled down and depressurized.

ASSOCIATED CONTENT

Supporting Information

The Supporting Information is available free of charge at https://pubs.acs.org/doi/10.1021/acsnano.2c04189.

Chemicals, characterization techniques, nanocrystal syntheses, PL spectra of CdSe NCs before and after ligand stripping and after irradiation, optical microscope images of patterned ZrO_2 and CdSe/CdS BF_4 NCs by mixing with ZnSe BF_4, SEM images of a patterned ZnSe NCs film, surface roughness of a ZnSe NC film before and after hot isostatic pressing, thick patterend ZnSe NC film, COMSOL modeling of the penetration depth of light into the ZnSe NC film, absorption spectra of oleate-capped NCs before and after irradiation, results of irradiation of ZnSe NCs in air and in air-free conditions, DLS spectra of ZnSe-BF_4 NCs upon irradiation, full FTIR spectra of ZnSe-BF_4 NC films after drying and/or irradiation, SEM images of NCs after polymer templating or hot isostatic pressing, and XRD diffraction patterns of ZnSe and ZnS NCs before and after hot isostatic pressing (PDF)

AUTHOR INFORMATION

Corresponding Author

Dmitri V. Talapin − *Department of Chemistry, James Franck Institute, and Pritzker School of Molecular Engineering, University of Chicago, Chicago, Illinois 60637, United States; Center for Nanoscale Materials, Argonne National Laboratory, Argonne, Illinois 60439, United States;* orcid.org/0000-0002-6414-8587; Email: dvtalapin@uchicago.edu

Authors

Jia-Ahn Pan − *Department of Chemistry, James Franck Institute, and Pritzker School of Molecular Engineering, University of Chicago, Chicago, Illinois 60637, United States;* orcid.org/0000-0001-6153-8611

Haoqi Wu − *Department of Chemistry, James Franck Institute, and Pritzker School of Molecular Engineering, University of Chicago, Chicago, Illinois 60637, United States*

Anthony Gomez − *Department of Chemistry, James Franck Institute, and Pritzker School of Molecular Engineering, University of Chicago, Chicago, Illinois 60637, United States*

Justin C. Ondry − *Department of Chemistry, James Franck Institute, and Pritzker School of Molecular Engineering, University of Chicago, Chicago, Illinois 60637, United States;* orcid.org/0000-0001-9113-3420

Joshua Portner − *Department of Chemistry, James Franck Institute, and Pritzker School of Molecular Engineering, University of Chicago, Chicago, Illinois 60637, United States*

Wooje Cho − *Department of Chemistry, James Franck Institute, and Pritzker School of Molecular Engineering, University of Chicago, Chicago, Illinois 60637, United States;* orcid.org/0000-0002-4022-4194

Alex Hinkle − *Department of Chemistry, James Franck Institute, and Pritzker School of Molecular Engineering, University of Chicago, Chicago, Illinois 60637, United States*

Di Wang − *Department of Chemistry, James Franck Institute, and Pritzker School of Molecular Engineering, University of Chicago, Chicago, Illinois 60637, United States*

Complete contact information is available at: https://pubs.acs.org/10.1021/acsnano.2c04189

Notes

The authors declare no competing financial interest.

ACKNOWLEDGMENTS

We thank Andrew Nelson for reading and revising the manuscript. We also thank Nanosys, Inc. (Milpitas, CA) for providing samples of colloidal InP QDs. This work was supported by the Department of Defense (DOD) Air Force Office of Scientific Research under Grant FA9550-18-1-0099 and by NSF under Award CHE-1905290. This work was also partially supported by the University of Chicago Materials Research Science and Engineering Center, which is funded by the National Science Foundation under Award DMR-2011854. Use of the Center for Nanoscale Materials, an Office of Science User Facilities operated for the U.S. Department of Energy (DOE) Office of Science by Argonne National Laboratory, was supported by the U.S. DOE under Contract DE-AC02-06CH11357. This work made use of the Pritzker Nanofabrication Facility, which receives partial support from the SHyNE Resource, a node of the National Science Foundation's National Nanotechnology Coordinated Infrastructure (Grant NSF ECCS-2025633).

REFERENCES

(1) Talapin, D. V.; Lee, J.-S.; Kovalenko, M. V.; Shevchenko, E. V. Prospects of Colloidal Nanocrystals for Electronic and Optoelectronic Applications. *Chem. Rev.* **2010**, *110* (1), 389−458.

(2) Garcia de Arquer, F. P.; Talapin, D. V.; Klimov, V. I.; Arakawa, Y.; Bayer, M.; Sargent, E. H. Semiconductor quantum dots: Technological progress and future challenges. *Science* **2021**, *373* (6555), eaaz8541.

(3) Kagan, C. R.; Lifshitz, E.; Sargent, E. H.; Talapin, D. V. Building devices from colloidal quantum dots. *Science* **2016**, *353* (6302), aac5523.

(4) Kim, J.; Kwon, S.-M.; Kang, Y. K.; Kim, Y.-H.; Lee, M.-J.; Han, K.; Facchetti, A.; Kim, M.-G.; Park, S. K. A skin-like two-dimensionally pixelized full-color quantum dot photodetector. *Sci. Adv.* **2019**, *5* (11), eaax8801.

(5) Cho, H.; Pan, J. A.; Wu, H.; Lan, X.; Coropceanu, I.; Wang, Y.; Cho, W.; Hill, E. A.; Anderson, J. S.; Talapin, D. V. Direct Optical Patterning of Quantum Dot Light-Emitting Diodes via In Situ Ligand Exchange. *Adv. Mater.* **2020**, *32* (46), 2003805.

(6) Yang, D.; Fuadi, M. K.; Kang, K.; Kim, D.; Li, Z.; Park, I. Multiplexed Gas Sensor Based on Heterogeneous Metal Oxide

Nanomaterial Array Enabled by Localized Liquid-Phase Reaction. *ACS Appl. Mater. Interfaces* **2015**, *7* (19), 10152−10161.
(7) Prins, F.; Kim, D. K.; Cui, J.; De Leo, E.; Spiegel, L. L.; McPeak, K. M.; Norris, D. J. Direct Patterning of Colloidal Quantum-Dot Thin Films for Enhanced and Spectrally Selective Out-Coupling of Emission. *Nano Lett.* **2017**, *17* (3), 1319−1325.
(8) Gheshlaghi, N.; Foroutan-Barenji, S.; Erdem, O.; Altintas, Y.; Shabani, F.; Humayun, M. H.; Demir, H. V. Self-Resonant Microlasers of Colloidal Quantum Wells Constructed by Direct Deep Patterning. *Nano Lett.* **2021**, *21*, 4598.
(9) Pan, J.-A.; Rong, Z.; Wang, Y.; Cho, H.; Coropceanu, I.; Wu, H.; Talapin, D. V. Direct Optical Lithography of Colloidal Metal Oxide Nanomaterials for Diffractive Optical Elements with 2π Phase Control. *J. Am. Chem. Soc.* **2021**, *143* (5), 2372−2383.
(10) Zhang, L.; Chao, D.; Yang, P.; Weber, L.; Li, J.; Kraus, T.; Fan, H. J. Flexible Pseudocapacitive Electrochromics via Inkjet Printing of Additive-Free Tungsten Oxide Nanocrystal Ink. *Adv. Energy Mater.* **2020**, *10* (17), 2000142.
(11) Liu, Y.; Li, F.; Qiu, L.; Yang, K.; Li, Q.; Zheng, X.; Hu, H.; Guo, T.; Wu, C.; Kim, T. W. Fluorescent Microarrays of in Situ Crystallized Perovskite Nanocomposites Fabricated for Patterned Applications by Using Inkjet Printing. *ACS Nano* **2019**, *13* (2), 2042−2049.
(12) Sliz, R.; Lejay, M.; Fan, J. Z.; Choi, M.-J.; Kinge, S.; Hoogland, S.; Fabritius, T.; García de Arquer, F. P.; Sargent, E. H. Stable Colloidal Quantum Dot Inks Enable Inkjet-Printed High-Sensitivity Infrared Photodetectors. *ACS Nano* **2019**, *13* (10), 11988−11995.
(13) Dieleman, C. D.; van der Burgt, J.; Thakur, N.; Garnett, E. C.; Ehrler, B. Direct Patterning of CsPbBr3 Nanocrystals via Electron-Beam Lithography. *ACS Applied Energy Materials* **2022**, *5* (2), 1672−1680.
(14) Miszta, K.; Greullet, F.; Marras, S.; Prato, M.; Toma, A.; Arciniegas, M.; Manna, L.; Krahne, R. Nanocrystal Film Patterning by Inhibiting Cation Exchange via Electron-Beam or X-ray Lithography. *Nano Lett.* **2014**, *14* (4), 2116−2122.
(15) Kim, T.-H.; Cho, K.-S.; Lee, E. K.; Lee, S. J.; Chae, J.; Kim, J. W.; Kim, D. H.; Kwon, J.-Y.; Amaratunga, G.; Lee, S. Y.; et al. Full-colour quantum dot displays fabricated by transfer printing. *Nat. Photonics* **2011**, *5* (3), 176.
(16) Kothari, R.; Beaulieu, M. R.; Hendricks, N. R.; Li, S.; Watkins, J. J. Direct Patterning of Robust One-Dimensional, Two-Dimensional, and Three-Dimensional Crystalline Metal Oxide Nanostructures Using Imprint Lithography and Nanoparticle Dispersion Inks. *Chem. Mater.* **2017**, *29* (9), 3908−3918.
(17) Yang, J.; Hahm, D.; Kim, K.; Rhee, S.; Lee, M.; Kim, S.; Chang, J. H.; Park, H. W.; Lim, J.; Lee, M.; Kim, H.; Bang, J.; Ahn, H.; Cho, J. H.; Kwak, J.; Kim, B.; Lee, C.; Bae, W. K.; Kang, M. S. High-resolution patterning of colloidal quantum dots via non-destructive, light-driven ligand crosslinking. *Nat. Commun.* **2020**, *11* (1), 2874.
(18) Kim, W. J.; Kim, S. J.; Lee, K.-S.; Samoc, M.; Cartwright, A. N.; Prasad, P. N. Robust microstructures using UV photopatternable semiconductor nanocrystals. *Nano Lett.* **2008**, *8* (10), 3262−3265.
(19) Hahm, D.; Park, J.; Jeong, I.; Rhee, S.; Lee, T.; Lee, C.; Chung, S.; Bae, W. K.; Lee, S. Surface Engineered Colloidal Quantum Dots for Complete Green Process. *ACS Appl. Mater. Interfaces* **2020**, *12* (9), 10563−10570.
(20) Pan, J.-A.; Ondry, J. C.; Talapin, D. V. Direct Optical Lithography of CsPbX3 Nanocrystals via Photoinduced Ligand Cleavage with Postpatterning Chemical Modification and Electronic Coupling. *Nano Lett.* **2021**, *21* (18), 7609−7616.
(21) Wang, Y.; Pan, J.-A.; Wu, H.; Talapin, D. V. Direct Wavelength-Selective Optical and Electron-Beam Lithography of Functional Inorganic Nanomaterials. *ACS Nano* **2019**, *13* (12), 13917−13931.
(22) Wang, Y.; Fedin, I.; Zhang, H.; Talapin, D. V. Direct optical lithography of functional inorganic nanomaterials. *Science* **2017**, *357* (6349), 385−388.
(23) Dong, A.; Ye, X.; Chen, J.; Kang, Y.; Gordon, T.; Kikkawa, J. M.; Murray, C. B. A generalized ligand-exchange strategy enabling sequential surface functionalization of colloidal nanocrystals. *J. Am. Chem. Soc.* **2011**, *133* (4), 998−1006.
(24) Nag, A.; Kovalenko, M. V.; Lee, J.-S.; Liu, W.; Spokoyny, B.; Talapin, D. V. Metal-free inorganic ligands for colloidal nanocrystals: S^{2-}, HS^{-}, Se^{2-}, HSe^{-}, Te^{2-}, HTe^{-}, TeS_3^{2-}, OH^{-}, and NH_2^{-} as surface ligands. *J. Am. Chem. Soc.* **2011**, *133* (27), 10612−10620.
(25) Rosen, E. L.; Buonsanti, R.; Llordes, A.; Sawvel, A. M.; Milliron, D. J.; Helms, B. A. Exceptionally mild reactive stripping of native ligands from nanocrystal surfaces by using Meerwein's salt. *Angew. Chem., Int. Ed.* **2012**, *51* (3), 684−689.
(26) Doris, S. E.; Lynch, J. J.; Li, C.; Wills, A. W.; Urban, J. J.; Helms, B. A. Mechanistic insight into the formation of cationic naked nanocrystals generated under equilibrium control. *J. Am. Chem. Soc.* **2014**, *136* (44), 15702−15710.
(27) Wang, W.; Pan, Z.; Rao, H.; Zhang, G.; Song, H.; Zhang, Z.; Zhong, X. Proton Initiated Ligand Exchange Reactions for Colloidal Nanocrystals Functionalized by Inorganic Ligands with Extremely Weak Coordination Ability. *Chem. Mater.* **2020**, *32* (1), 630−637.
(28) Maenosono, S.; Ozaki, E.; Yoshie, K.; Yamaguchi, Y. Nonlinear Photoluminescence Behavior in Closely Packed CdSe Nanocrystal Thin Films. *Jpn. J. Appl. Phys.* **2001**, *40* (Part 2, No. 6B), L638−L641.
(29) Manner, V. W.; Koposov, A. Y.; Szymanski, P.; Klimov, V. I.; Sykora, M. Role of Solvent−Oxygen Ion Pairs in Photooxidation of CdSe Nanocrystal Quantum Dots. *ACS Nano* **2012**, *6* (3), 2371−2377.
(30) Dunstan, D. E.; Hagfeldt, A.; Almgren, M.; Siegbahn, H. O.; Mukhtar, E. Importance of surface reactions in the photochemistry of zinc sulfide colloids. *J. Phys. Chem.* **1990**, *94* (17), 6797−6804.
(31) Spanhel, L.; Haase, M.; Weller, H.; Henglein, A. Photochemistry of colloidal semiconductors. 20. Surface modification and stability of strong luminescing CdS particles. *J. Am. Chem. Soc.* **1987**, *109* (19), 5649−5655.
(32) Wang, F.; Yu, H.; Li, J.; Hang, Q.; Zemlyanov, D.; Gibbons, P. C.; Wang; Janes, D. B.; Buhro, W. E. Spectroscopic Properties of Colloidal Indium Phosphide Quantum Wires. *J. Am. Chem. Soc.* **2007**, *129* (46), 14327−14335.
(33) Janke, E. M.; Williams, N. E.; She, C.; Zherebetskyy, D.; Hudson, M. H.; Wang, L.; Gosztola, D. J.; Schaller, R. D.; Lee, B.; Sun, C.; Engel, G. S.; Talapin, D. V. Origin of Broad Emission Spectra in InP Quantum Dots: Contributions from Structural and Electronic Disorder. *J. Am. Chem. Soc.* **2018**, *140* (46), 15791−15803.
(34) Adam, S.; Talapin, D. V.; Borchert, H.; Lobo, A.; McGinley, C.; de Castro, A. R. B.; Haase, M.; Weller, H.; Möller, T. The effect of nanocrystal surface structure on the luminescence properties: Photoemission study of HF-etched InP nanocrystals. *J. Chem. Phys.* **2005**, *123* (8), 084706.
(35) Srivastava, S.; Santos, A.; Critchley, K.; Kim, K.-S.; Podsiadlo, P.; Sun, K.; Lee, J.; Xu, C.; Lilly, G. D.; Glotzer, S. C.; Kotov, N. A. Light-Controlled Self-Assembly of Semiconductor Nanoparticles into Twisted Ribbons. *Science* **2010**, *327* (5971), 1355−1359.
(36) Rivest, J. B.; Buonsanti, R.; Pick, T. E.; Zhu, L.; Lim, E.; Clavero, C.; Schaible, E.; Helms, B. A.; Milliron, D. J. Evolution of Ordered Metal Chalcogenide Architectures through Chemical Transformations. *J. Am. Chem. Soc.* **2013**, *135* (20), 7446−7449.
(37) Buonsanti, R.; Pick, T. E.; Krins, N.; Richardson, T. J.; Helms, B. A.; Milliron, D. J. Assembly of Ligand-Stripped Nanocrystals into Precisely Controlled Mesoporous Architectures. *Nano Lett.* **2012**, *12* (7), 3872−3877.
(38) Rauda, I. E.; Buonsanti, R.; Saldarriaga-Lopez, L. C.; Benjauthrit, K.; Schelhas, L. T.; Stefik, M.; Augustyn, V.; Ko, J.; Dunn, B.; Wiesner, U.; Milliron, D. J.; Tolbert, S. H. General Method for the Synthesis of Hierarchical Nanocrystal-Based Mesoporous Materials. *ACS Nano* **2012**, *6* (7), 6386−6399.
(39) Rauda, I. E.; Saldarriaga-Lopez, L. C.; Helms, B. A.; Schelhas, L. T.; Membreno, D.; Milliron, D. J.; Tolbert, S. H. Nanoporous Semiconductors Synthesized Through Polymer Templating of Ligand-Stripped CdSe Nanocrystals. *Adv. Mater.* **2013**, *25* (9), 1315−1322.
(40) Ondry, J. C.; Robbennolt, S.; Kang, H.; Yan, Y.; Tolbert, S. H. A Room-Temperature, Solution Phase Method for the Synthesis of Mesoporous Metal Chalcogenide Nanocrystal-Based Thin Films with

https://doi.org/10.1021/acsnano.2c04189
ACS Nano 2022, 16, 16067−16076

Precisely Controlled Grain Sizes. *Chem. Mater.* **2016**, *28* (17), 6105−6117.
(41) Gupta, R.; Goddard, N. J. Broadband absorption spectroscopy for rapid pH measurement in small volumes using an integrated porous waveguide. *Analyst* **2017**, *142* (1), 169−176.
(42) Girault, P.; Lorrain, N.; Lemaitre, J.; Poffo, L.; Guendouz, M.; Hardy, I.; Gadonna, M.; Gutierrez, A.; Bodiou, L.; Charrier, J. Racetrack micro-resonators based on ridge waveguides made of porous silica. *Opt. Mater.* **2015**, *50*, 167−174.
(43) Burgess, I. B.; Koay, N.; Raymond, K. P.; Kolle, M.; Lončar, M.; Aizenberg, J. Wetting in Color: Colorimetric Differentiation of Organic Liquids with High Selectivity. *ACS Nano* **2012**, *6* (2), 1427−1437.
(44) Singleton, T. A.; Burgess, I. B.; Nerger, B. A.; Goulet-Hanssens, A.; Koay, N.; Barrett, C. J.; Aizenberg, J. Photo-tuning of highly selective wetting in inverse opals. *Soft Matter* **2014**, *10* (9), 1325−1328.
(45) Campo, A. d.; Greiner, C. SU-8: a photoresist for high-aspect-ratio and 3D submicron lithography. *Journal of Micromechanics and Microengineering* **2007**, *17* (6), R81−R95.
(46) Hellgren, N.; Steves, M. A.; Shallenberger, J.; O'Boyle, S. K.; Mellott, E.; Noble, A. R. Effect of etching on the oxidation of zinc selenide surfaces characterized by X-ray photoelectron spectroscopy. *Appl. Surf. Sci.* **2020**, *528*, 146604.
(47) Dabbousi, B. O.; Rodriguez-Viejo, J.; Mikulec, F. V.; Heine, J. R.; Mattoussi, H.; Ober, R.; Jensen, K. F.; Bawendi, M. G. (CdSe)ZnS Core−Shell Quantum Dots: Synthesis and Characterization of a Size Series of Highly Luminescent Nanocrystallites. *J. Phys. Chem. B* **1997**, *101* (46), 9463−9475.
(48) Atkinson, H. V.; Davies, S. Fundamental aspects of hot isostatic pressing: An overview. *Metallurgical and Materials Transactions A* **2000**, *31* (12), 2981−3000.
(49) Braun, M. M.; Pilon, L. Effective optical properties of non-absorbing nanoporous thin films. *Thin Solid Films* **2006**, *496* (2), 505−514.
(50) Garahan, A.; Pilon, L.; Yin, J.; Saxena, I. Effective optical properties of absorbing nanoporous and nanocomposite thin films. *J. Appl. Phys.* **2007**, *101* (1), 014320.

https://doi.org/10.1021/acsnano.2c04189
ACS Nano 2022, 16, 16067−16076